J. Fluid Mech. (2011), *vol.* 689, *pp.* 552–563.
doi:10.1017/jfm.2011.453

Pulsating electrohydrodynamic cone-jets: from choked jet to oscillating cone

David B. Bober and Chuan-Hua Chen†

Department of Mechanical Engineering and Materials Science, Duke University, Durham, NC 27708, USA

(Received 1 May 2011; revised 2 September 2011; accepted 13 October 2011; first published online 14 November 2011)

Pulsating cone-jets occur in a variety of electrostatic spraying and printing systems. This paper reports an experimental study of the pulsation frequency to reconcile two models based on a choked jet and an oscillating cone, respectively. The two regimes are demarcated by the ratio of the supplied flow rate (Q_s) to the minimum flow rate (Q_m) required for a steady Taylor cone-jet. When $Q_s \lesssim Q_m$, the electrohydrodynamic flow is choked at the nozzle because the intermittent jet, when on, emits mass at the minimum flow rate; the pulsation frequency in the choked jet regime is proportional to Q_s/Q_m. When $Q_s \gtrsim Q_m$, the Taylor cone anchored at the nozzle experiences a capillary oscillation analogous to the Rayleigh mode of a free drop; the pulsation frequency in the oscillating cone regime plateaus to the capillary oscillation frequency, which is independent of Q_s/Q_m.

Key words: electrohydrodynamic effects

1. Introduction

Electrohydrodynamic cone-jets have wide-ranging applications for the production of ions, particles and fibres through electrostatic spraying, printing and spinning. Although a steady cone-jet is preferred in many applications, pulsating cone-jets are frequently encountered, particularly in low-flow-rate systems such as miniaturized electrospraying (nanoelectrospray) (Wilm & Mann 1994; Lu *et al.* 2001; Alexander, Paine & Stark 2006) and fine-resolution electrohydrodynamic printing (Yogi *et al.* 2001; Chen, Saville & Aksay 2006*a*; Park *et al.* 2007). Pulsating cone-jets are typically quasi-steady for the duration of jetting, and are therefore closely related to steady cone-jets (Fernandez de la Mora 1996, 2007). Cone-jet pulsations can occur intrinsically under steady operating conditions, or be triggered externally, e.g. by a pulsed voltage (Juraschek & Rollgen 1998; Wei *et al.* 2002). The former is usually called 'intrinsic (unforced, natural) pulsation', while the latter is called 'external (forced, imposed) pulsation'. Note that intrinsic pulsations can also occur with externally pulsed voltages of long enough duration (Chen, Saville & Aksay 2006*b*; Stachewicz *et al.* 2009).

In this paper, we focus on the intrinsic pulsations with a constant external voltage. We further restrict our attention to the parametric regime in which a single jet

† Email address for correspondence: chuanhua.chen@duke.edu

periodically forms and vanishes at a single frequency, i.e. the 'axial mode II' in Juraschek & Rollgen (1998). Although we have also observed other modes, including those discussed by Juraschek & Rollgen (1998), the single-jet, single-frequency mode is the most important one in terms of practical applications in designing high-resolution electroprinting (Chen *et al.* 2006*a*; Park *et al.* 2007) and improving electrospray efficiencies (Lu *et al.* 2001; Alexander *et al.* 2006). The single-frequency pulsation mode is also the simplest to model owing to its close relation to the well-studied steady cone-jet.

The theme of this paper is to reconcile two types of models for the frequency of intrinsic pulsations. One model is based on the free oscillation of the conical meniscus (Rayleigh 1882; Marginean *et al.* 2006); the other is based on the imbalance of mass flow supplied to the cone and emitted by the jet (Fernandez de la Mora 1996; Chen *et al.* 2006*b*). We will show that each model is valid within its applicable regime of flow rates. This work will hopefully be a step towards reconciling numerous models proposed for pulsating cone-jets, e.g. those in recent work by Choi *et al.* (2008), Paine (2009) and Stachewicz *et al.* (2010).

2. Theoretical models

On the voltage–flow rate (V–Q) operating diagram, there is a stability island for the steady cone-jet (see Cloupeau & Prunet-Foch 1989; Fernandez de la Mora 2007; Chen 2011, among others); see figure 3 below. To form a steady cone-jet, a minimum flow rate (Q_m) is required to sustain the steady jet. At Q_m, the Taylor voltage (V_m) leads to a steady cone-jet (Taylor 1964). At each flow rate above Q_m, there is a range of voltages around V_m that yields a steady cone-jet. In this paper, we are mainly concerned with the cone-jet pulsation modes at voltages *below the Taylor voltage* ($V < V_m$).

The minimum flow rate empirically scales as (see Fernandez de la Mora & Loscertales 1994; Ganan-Calvo, Davila & Barrero 1997; Fernandez de la Mora 2007, among others)

$$Q_m \sim \frac{\gamma \varepsilon}{\rho \sigma}, \tag{2.1}$$

where γ is the surface tension, ε is the dielectric permittivity, ρ is the density and σ is the conductivity of the working liquid. The Q_m scaling is reported to work well for working fluids of relatively high conductivity ($\sigma \gtrsim 1$ μS cm^{-1}) (Fernandez de la Mora 2007).

With the voltage below the Taylor voltage but large enough for transient cone-jets to form, the oscillation modes of pulsating cone-jets can be demarcated by the flow rate ratio (Q_s/Q_m). When $Q_s \gtrsim Q_m$, the entire cone oscillates with ample supply of liquid to the cone, and the pulsating jet has the same frequency as the intrinsic frequency of conical oscillation (Marginean *et al.* 2006). When $Q_s \lesssim Q_m$, the conical base stays more or less unperturbed, and the pulsating jet results because of insufficient upstream supply of liquid to the downstream jet (Chen *et al.* 2006*b*). Although in this study we have restricted the voltage to be below the Taylor voltage to avoid multi-jets, it helps to envision both modes with a voltage exactly at the Taylor voltage: insufficient flow rate still results in a pulsating jet (which is a choked jet), while sufficient flow rate results in a steady cone-jet (instead of an oscillating cone).

When $Q_s \gtrsim Q_m$ but $V < V_m$, the cone-jet pulsation is in the 'oscillating cone' regime. The entire cone oscillates at a frequency that follows a similar scaling law governing the free (Rayleigh) oscillation of a charged drop (Marginean *et al.* 2006). For an isolated drop with a diameter d, the most unstable resonance mode is $f = (4/\pi)\sqrt{1 - q^2/q_R^2}\sqrt{\gamma/(\rho d^3)}$, where q is the total surface charge and $q_R = \sqrt{8\pi^2\varepsilon_0\gamma d^3}$ is the electrostatic Rayleigh limit (Rayleigh 1882), with ε_0 denoting the permittivity of the surrounding gas. For the Taylor cone, the surface charge is controlled in part by the applied voltage. Mainly concentrated at the conical apex, the surface charge (and therefore q/q_R) integrated over the entire conical surface and averaged over a full period of oscillation should be approximately constant. With this simplification, the frequency of the oscillating cone is primarily mechanical in nature,

$$f \sim \sqrt{\frac{\gamma}{\rho d^3}} = f_c, \tag{2.2}$$

where d is the anchoring diameter of the nozzle (e.g. inner diameter for non-wetting nozzle, and outer diameter for wetting nozzle), and f_c is the capillary frequency.

When $Q_s \lesssim Q_m$, the cone-jet pulsation is in the 'choked jet' regime for voltages both above and below V_m, but the discussion here is restricted to $V < V_m$. In this regime, the conical apex can only periodically emit a jet because the supplied flow rate is smaller than what a steady jet needs to carry (Chen *et al.* 2006*b*). The pulsating cone-jet issued from a nozzle is analogous to that on an isolated drop reaching the Rayleigh limit (q_R) (Fernandez de la Mora 1996). On a charged drop, a transient jet results when the surface charge q is above q_R and the excessive charge has to be redistributed to a larger surface area (via a Taylor cone-jet). Based on studies of isolated drops, the charge loss ratio $\Delta q/q_R$ is approximately constant (typically larger than 10 %) for a given working fluid and is much larger than the mass loss ratio $\Delta m/m$ (Fernandez de la Mora 1996). Analogously, the charge loss process from the cone stipulates the jetting duration (Δt), which is given by the time required to eject enough charge (Δq) in order to arrive at a new electrostatic equilibrium (Fernandez de la Mora 1996),

$$\Delta t \sim \frac{\Delta q}{I} \sim \frac{q_R}{I} \sim \frac{\sqrt{\varepsilon_0\gamma d^3}}{\sqrt{\varepsilon_0\gamma^2/\rho}} \sim \sqrt{\frac{\rho d^3}{\gamma}} = t_c, \tag{2.3}$$

where $I \sim g(\varepsilon)\sqrt{\varepsilon_0\gamma^2/\rho}$ is the current carried by the jet with $g(\varepsilon)$ ($\approx$18 for ethylene glycol and water) accounting for the effect of liquid permittivity (Fernandez de la Mora & Loscertales 1994), and $t_c = 1/f_c$ is the capillary time. Although the jetting duration is stipulated by the electrostatic discharging process, the jetting frequency (and duty cycle) is governed by the imbalance of mass flow. The emitted surface charge can be replenished from bulk ions, which are abundant locally within the cone for a high-conductivity liquid, but the emitted mass has to be eventually supplied from upstream. Within a full period (T) of pulsation, the upstream supply of Q_sT balances the downstream emission of $Q_m\Delta t$ (Chen *et al.* 2006*b*), leading to

$$f = \frac{1}{T} \sim \frac{Q_s}{Q_m\Delta t} \sim \frac{Q_s}{Q_m t_c} \sim \frac{Q_s}{Q_m} f_c. \tag{2.4}$$

In summary, the regimes of choked jet and oscillating cone are demarcated by the ratio of the supplied to the minimum flow rate (Q_s/Q_m),

$$f \sim \begin{cases} \dfrac{Q_s}{Q_m} f_c, & \text{if } \dfrac{Q_s}{Q_m} \lesssim 1, \\ f_c, & \text{if } \dfrac{Q_s}{Q_m} \gtrsim 1. \end{cases} \tag{2.5}$$

Interestingly, Q_s/Q_m also appears as a prefactor in the pulsation frequency, which ensures a smooth transition from the choked jet regime to the oscillating cone regime. This scaling model is alternatively justified by a dimensional analysis in the Appendix, where the analysis also suggests the parametric regime of validity for (2.5).

3. Experimental methods

The electrohydrodynamic cone-jet pulsations were produced on an electrified glass nozzle. The uncoated, tapered nozzle had an inner diameter of 100 μm, and an outer diameter of 150 μm at the nozzle exit (New Objective TT360-100-50-N-5). The nozzle was cut to a length of 3.6 mm and fixed to a stainless steel union (via a tubing sleeve). The metallic union was grounded with respect to a negatively electrified planar electrode (Trek 610E), and the voltage was 2.1 kV unless otherwise specified (the voltage varied in figure 3). The electrode was made of textured silicon (Zhao *et al.* 2009) to help spread the working fluid, and was held 1 mm apart from the nozzle exit. The flow rate was externally imposed by a syringe pump (KD Scientific 100 or Legato 180).

The working fluid was ethylene glycol (CAS No. 107-21-1) doped with sodium borate (CAS No. 1303-96-4) to an appropriate conductivity (measured with an Oakton 510). The conductivity (σ) was 3.6×10^{-4} S m^{-1} unless otherwise noted. Based on the literature properties of pure ethylene glycol at room temperature, the viscosity (μ) is 1.6×10^{-2} Pa s, density (ρ) is 1.1×10^{3} kg m^{-3}, surface tension (γ) is 4.8×10^{-2} N m^{-1} and permittivity (ε) is 3.3×10^{-10} C V^{-1} m.

The pulsation frequency was measured by an oscilloscope and confirmed by a high-speed camera. The 100 MHz oscilloscope (Agilent DS05014A) was connected in series with the electrohydrodynamic jet, and the current was measured from the voltage drop on the standard 1 MΩ resistance of the oscilloscope. Electrical noise was minimized with a Faraday cage. In addition, the high-voltage supply was filtered with a low-pass *RC* circuit to eliminate high-frequency noise. High-speed video of the cone-jet pulsation was captured at 1.50×10^{5} frames per second (f.p.s.) by a Phantom v710 camera via an Infinity K2 microscope. The high frame rate enabled measurement of the jetting duration. Illumination was provided by a light-emitting diode (LED) light source (Fiber-Lite LMI-8000) to minimize heating. Although the oscilloscopic and imaging measurements yielded identical frequencies, the former was adopted for convenience unless otherwise specified, and video imaging was primarily used to spot-check the accuracy of the current measurements.

4. Results and discussion

The flow rate was used as the main control parameter to study the pulsation frequency. In figure 1, a series of high-speed videos were captured from pulsating cone-jets at different flow rates. The corresponding measurements in table 1 indicate that, with increasing flow rates, the pulsation frequency first increased rapidly at lower

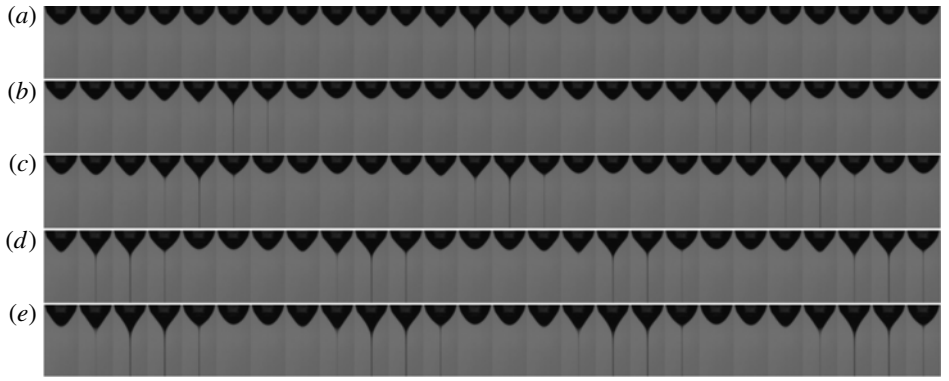

FIGURE 1. Cone-jet pulsations at increasing flow rates detailed in table 1, with the flow rate doubling in each row: (*a*,*b*) choked jet regime, in which the frequency increased approximately linearly with increasing flow rate; (*c*) transition regime; and (*d*,*e*) oscillating cone regime, in which the frequency was approximately constant. Each individual image averages six adjacent video frames captured at 1.50×10^5 f.p.s., i.e. each image represents a duration of 40 μs with a dimension of 180 μm × 370 μm.

	Flow rate, Q_s (nl s^{-1})	Frequency, f (Hz)	Duration, Δt (μs)	Duty cycle, $f\Delta t$ (%)	Reduced rate, Q_s/Q_m	Pulsation regime
(*a*)	2.8	994	87	8.6	0.5	choked jet
(*b*)	5.6	1780	87	15.5	0.9	choked jet
(*c*)	11.1	2780	95	26.4	2	transitional
(*d*)	22.2	3410	113	38.5	4	oscillating cone
(*e*)	44.4	3590	142	51.1	7	oscillating cone

TABLE 1. Flow rates and the associated measurements corresponding to figure 1. The frequency and duration were measured from video imaging. The minimum flow rate of $Q_m \approx 6$ nl s^{-1} is taken as that measured in figure 3. Note that the regimes of choked jet and oscillating cone are demarcated by $Q_s/Q_m \sim 1$.

flow rates and then approached a plateau value at higher flow rates. Note that the jetting duration was significantly longer than the charge relaxation time of 0.9 μs for ethylene glycol with a conductivity of 3.6 μS cm^{-1}. The rapid charge relaxation process ensures the validity of the quasi-steady assumption implied in (2.3).

The trend of frequency versus flow rate measured by video imaging (figure 1) was confirmed by oscilloscopic measurements of the current (figure 2). The plateau frequency of around 3500 Hz measured at high flow rates is very close to the capillary oscillation frequency predicted by (2.2), which yields 3600 Hz for ethylene glycol with a diameter of 150 μm. The good agreement is in part due to the close resemblance of the capillary frequency scaling to the exact Rayleigh solution.

A common problem in reproducing electrohydrodynamic results is the notorious difficulty in reproducing geometrical conditions that would influence the electrostatic field and consequently the electrohydrodynamic flow. Throughout figures 2–4 we have used the same geometrical set-up, i.e. with the same nozzle, metallic union and ground electrode left unchanged in the Faraday cage. The error bars of our measurement should be understood with this constraint in mind. Unfortunately, we had to replace

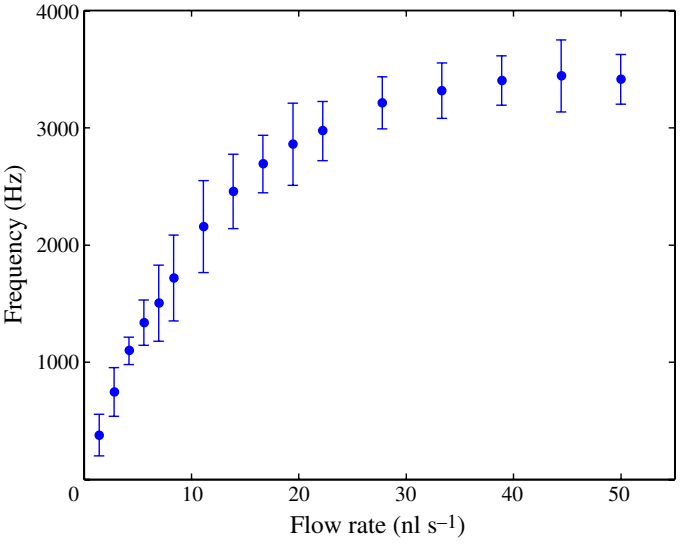

FIGURE 2. (Colour online available at journals.cambridge.org/flm) In the choked jet regime, with smaller flow rates, the pulsation frequency increases with flow rate. In the oscillating cone regime, at larger flow rates, the frequency plateaus to an approximately constant value. The error bars correspond to the 95 % confidence intervals of independent realizations on three different days.

the nozzle before figure 1 could be captured, although we tried our best to put the nozzle back to the original location. As a result, some frequencies measured in figure 1 were slightly outside the 95 % confidence intervals reported in figure 2.

The data in figures 1 and 2 indicate two distinct operating regimes in accordance with (2.5): choked jet at 'low' flow rates and oscillating cone at 'high' flow rates. At low flow rates, the pulsation frequency f almost doubled with doubling flow rate Q_s (figure 1*a–b*), which agrees with (2.4). In the choked jet regime, the jetting duration Δt was approximately constant, which agrees with (2.3), and larger flow rates were accommodated by higher frequencies (i.e. longer duty cycles). At high flow rates, the pulsation frequency was approximately constant (figure 2), which agrees with (2.2). In the oscillating cone regime, higher flow rates were accommodated by a combination of longer duty cycles and thicker jets.

The demarcation between the two pulsation regimes is best shown on the voltage–flow rate (V–Q_s) operating diagram (figure 3). The V–Q_s diagram experimentally defines the minimum flow rate (Q_m) and the approximate Taylor voltage (V_m) required to sustain a steady jet. Extracting from the stability island in figure 3, $Q_m \approx 6.3$ nl s^{-1} and $V_m \approx 2.9$ kV. As shown below, Q_m is the benchmark against which 'low' and 'high' flow rates are defined.

The measurement of the minimum flow rate is somewhat affected by the criteria used to define the stability island, but the order of magnitude of Q_m is not affected in our experience. We systematically searched the stability island by incrementally decreasing the flow rate, and gradually increasing the voltage at each given flow rate. By ensuring that the voltage was monotonically increased, we avoided the well-known hysteresis of the stability island (Cloupeau & Prunet-Foch 1989) if voltage were to change in both directions. The lower bound of the stability island corresponded to the

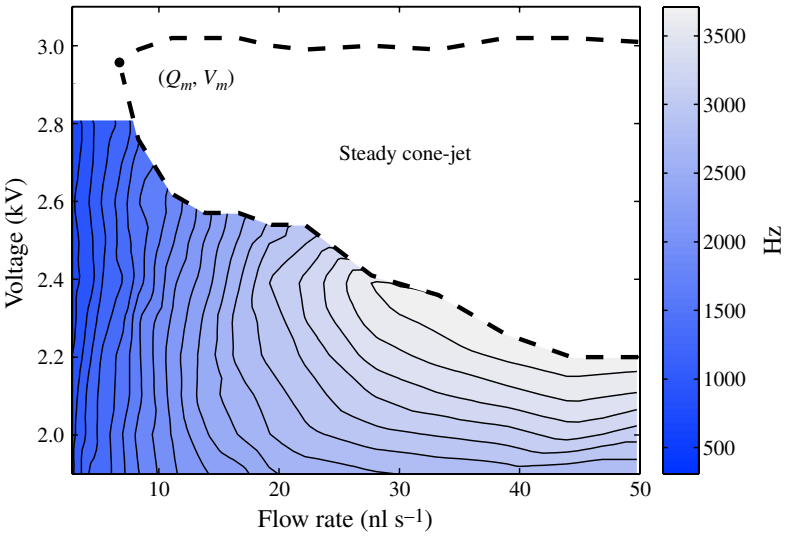

FIGURE 3. (Colour online) Frequency contours overlaid on the V–Q_s operating diagram, which defines the minimum flow rate (Q_m) required to produce a steady cone-jet. At Q_m, a steady cone-jet is produced at the Taylor voltage (V_m). When the supplied flow rate (Q_s) is below Q_m, the frequency is a strong function of flow rate, with nearly vertical contour lines. When Q_s is above Q_m, the frequency becomes a weak function of flow rate, with nearly horizontal contour lines. At a given voltage, a plot similar to figure 2 can be obtained from the frequency contours.

first appearance of a steady jet, and the upper bound to the first appearance of (an) unstable jet(s).

The specific criteria for the stability island were chosen to minimize the uncertainty in experimentally extracting Q_m. The lower bound was complicated by the astable regime in which a jet randomly fluctuates between a quasi-steady and a pulsating state (Marginean, Nemes & Vertes 2007). Fortunately, the astable regime had a very limited parametric range and its effect diminished close to the minimum flow rate. The upper bound was complicated by the many possible modes for a steady jet to become unstable (Cloupeau & Prunet-Foch 1994). However, when we consistently searched for the first unstable jet whose location on the nozzle fluctuated with time, the upper bound was well defined, particularly for flow rates close to Q_m.

Figure 3 also helps to define the V–Q_s parametric space we explored. We did not explore extremely low flow rates, which give rise to multiple-frequency pulsations, e.g. bursting modes with multiple distinct frequencies (Juraschek & Rollgen 1998) or even aperiodic events. The large uncertainty in frequency measurements at low flow rates (figure 4*a*) is a strong indication that the flow rate is approaching the boundary of the single-frequency pulsation regime. Although smaller nozzles (particularly tapered ones) are known to accommodate lower flow rates (Chowdhury & Chait 1991; Wilm & Mann 1994), consistent and non-clogging external pumping was challenging to accomplish for nozzles with an inner diameter of 10 μm or less. We did not explore extremely high flow rates, which give rise to an essentially hydrodynamic jet. At intermediate flow rates, the frequencies were only measured for voltages below V_m, the onset conditions for a steady jet (Taylor 1964). Above V_m, it was difficult to consistently obtain single-frequency, single-jet pulsations.

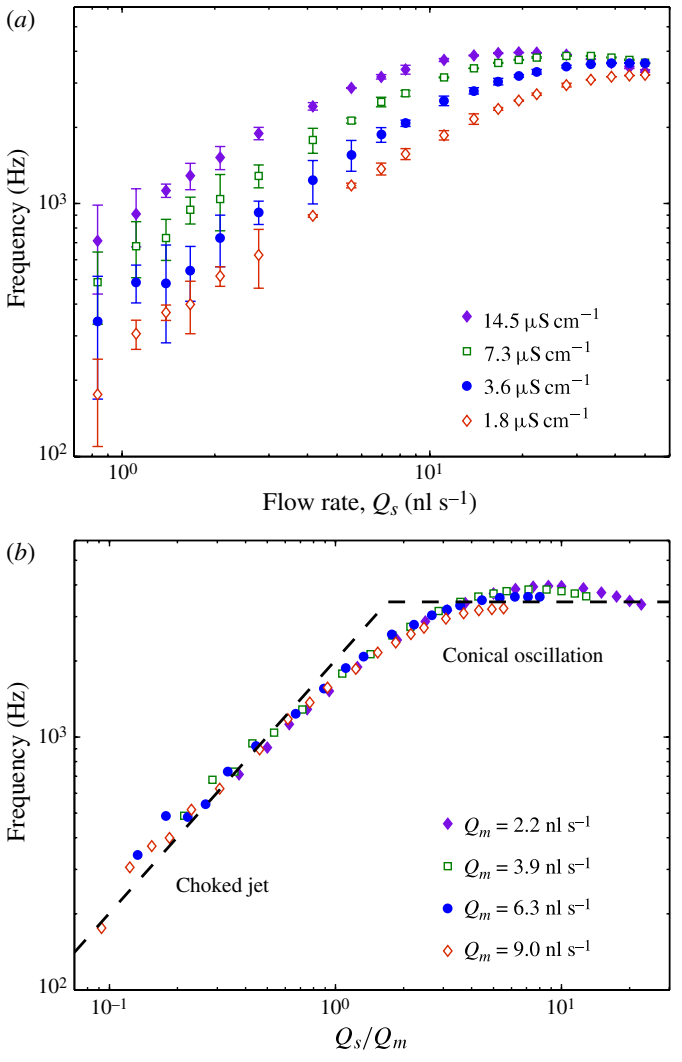

FIGURE 4. (Colour online) (*a*) For ethylene glycol with conductivities (σ) spanning an order of magnitude, the pulsation frequency at increasing flow rates follows the same trend. (*b*) The data are collapsed onto a single curve with the supplied flow rate (Q_s) normalized by the *measured* minimum flow rate (Q_m). The slope 1 and slope 0 lines signify the choked jet and oscillating cone regimes, respectively. The transition between the two regimes occurs around $Q_s/Q_m \sim 1$, with the measured Q_m approximately following the σ^{-1} scaling trend predicted by (2.1).

Frequency contours are overlaid on the V–Q_s operating diagram in figure 3. These frequencies were measured in a similar fashion to figure 2 over a range of voltages. Two pulsation regimes are apparent: at low flow rates ($Q_s \lesssim Q_m$), the frequency contours are nearly vertical lines, showing the strong dependence of the pulsation frequency on the imposed flow rate (choked jet regime); at high flow rates ($Q_s \gtrsim Q_m$), the frequency contours are more like horizontal lines, showing the much weaker dependence on the flow rate (oscillating cone regime). Note that the choked jet regime had very weak dependence on the voltage. In contrast, the oscillating cone regime had

a stronger dependence on voltage, which has been reported in other studies (Juraschek & Rollgen 1998; Parvin *et al.* 2005); see also the discussions on the electric Bond number in the Appendix.

To confirm that the minimum flow rate was indeed demarcating the regimes of choked jet and oscillating cone, we changed the conductivity by an order of magnitude while holding other liquid properties constant. For each of the four conductivities (see legend in figure 4*a*), the minimum flow rate was measured following procedures described in figure 3. The measured Q_m (figure 4*b*) followed the scaling trend in (2.1) that Q_m is inversely proportional to conductivity, although the dependence was somewhat weaker than σ^{-1}. Within the conductivity range we tested, the measured Q_m was consistently 10–20 % of that predicted by (2.1).

The pulsation frequency was measured as a function of the imposed flow rate at a fixed voltage of 2.1 kV (figure 4). In figure 4(*a*), all four curves qualitatively resembled the trend observed earlier in figure 2. When the imposed flow rate Q_s was normalized by the *measured* Q_m in figure 4(*b*), all four curves collapsed onto a master curve. The collapsed curve is well predicted by (2.5), which combines the two pulsation regimes. In the log–log plot, the choked jet regime approaches the slope 1 line at low flow rates, while the oscillating cone regime approaches the slope 0 line at high flow rates. The transition from the choked jet to the oscillating cone regime occurred when the supplied flow rate was approximately equal to the minimum flow rate.

In addition to ethylene glycol, both the choked jet and oscillating cone regimes have been shown for aqueous solutions with conductivities above 1 μS cm^{-1} or so (Chen *et al.* 2006*b*; Marginean *et al.* 2006; Xu 2010). For working fluids with a low viscosity (e.g. water), care has to be taken to avoid exciting the oscillating cone mode even when $Q_s < Q_m$; a non-wetting nozzle is much better than a wetting one for this purpose (Xu 2010; Chen 2011). For highly viscous fluids, e.g. glycerol that we experimentally tested, the minimum flow rate scaling equation (2.1) is no longer valid, nor is the frequency scaling equation (2.5); see also the discussions on the Ohnesorge number in the Appendix.

A note is warranted here about the nozzle, which was made of glass with a fixed diameter in this report. Prior work by Marginean *et al.* (2006) and Xu (2010) provided solid evidence for the scaling of the capillary oscillation frequency ($f \propto d^{-3/2}$) using both tapered and blunt nozzles of various diameters. In addition to the 150 μm tapered nozzles reported above, we verified that the minimum flow rate indeed demarcated the choked jet and oscillating cone regimes, using both water in flush-cut Teflon nozzles with an inner diameter of 50 μm (see also Chen *et al.* 2006*b*) and ethylene glycol in tapered glass nozzles with an outer diameter of 30 μm. Our model implies that the jet diameter is significantly smaller than the nozzle (cone) diameter, an assumption no longer valid when the nozzle diameter approaches the (typically micrometric) jet diameter.

5. Conclusion

The single-jet, single-frequency electrohydrodynamic cone-jet pulsation can be divided into the choked jet and oscillating cone regimes. On the voltage–flow rate operating diagram (figure 3), both regimes studied here fall below the Taylor voltage (V_m) required to initiate a steady jet. The two regimes are demarcated by the ratio of the supplied flow rate (Q_s) to the minimum flow rate (Q_m) required to sustain a steady jet. When $Q_s/Q_m \lesssim 1$, the pulsation is in the choked jet regime with $f \sim (Q_s/Q_m)f_c$,

where f_c is the capillary oscillation frequency of the cone. When $Q_s/Q_m \gtrsim 1$, the pulsation is in the oscillating cone regime with $f \sim f_c$, which is independent of flow rate. Our results are particularly relevant to electrohydrodynamic printing and miniaturized electrospraying, where low flow rates prohibit a steady cone-jet, resulting in pulsations in the choked jet regime.

Our work has strong implications for understanding cone-jet pulsations in the single-jet, single-frequency regime, the pulsation mode of arguably the most practical use. With (2.5) reconciling two existing models (Chen *et al.* 2006*b*; Marginean *et al.* 2006), the operating regime and pulsation frequency can be quickly estimated from a knowledge of the liquid properties and the wetted nozzle diameter. The liquid properties can be used to estimate Q_m using (2.1), particularly at relatively high conductivities and low viscosities, and the nozzle diameter can used to estimate f_c using (2.2). If the minimum flow rate can be experimentally measured, the frequency at a given Q_s/Q_m can be more accurately determined from a master curve similar to figure 4(*b*), which can be fixed by a few selected measurements.

Acknowledgements

This work was supported by an NSF CAREER Award (CBET-08-46705). We thank F. Liu, W. Scheideler and Y. Zhao for helpful discussions, and M. Chiang and S. Xu for their work during the initial phase of this project.

Appendix. Dimensional analysis

In this appendix, we use dimensional analysis to justify our scaling model of the pulsation frequency, (2.5). Despite a few noteworthy limitations, the dimensional analysis is particularly useful for identifying the regime of validity for our model.

For a pulsating cone-jet, the fundamental frequency of oscillation (f) depends on the following variables:

$$f = f(\rho, \gamma, \varepsilon, \sigma, \mu, \varepsilon_0, d, L, V, Q_s), \tag{A 1}$$

where ρ, γ, ε, σ and μ are, respectively, the density, surface tension, permittivity, conductivity and viscosity of the liquid, ε_0 is the permittivity of the surrounding air, d is the diameter of the nozzle, L is the separation between the nozzle and the counter-electrode, V is the applied voltage and Q_s is the supplied flow rate. Here, the hydrodynamic effects of the outer air are neglected, and the surrounding air only enters into the problem electrostatically as a dielectric medium. By dimensional analysis, (A 1) can be reduced to

$$\frac{f}{f_c} = F_1\left(\frac{\varepsilon}{\varepsilon_0}, \frac{t_e}{t_c}, \frac{\mu}{\sqrt{\rho\gamma d}}, \frac{L}{d}, \frac{\varepsilon_0 V^2}{\gamma d}, \frac{Q_s}{Q_m}\right), \tag{A 2}$$

where $f_c = \sqrt{\gamma/(\rho d^3)}$ is the capillary inertial frequency, $t_e = \varepsilon/\sigma$ is the charge relaxation time, $t_c = 1/f_c$ is the capillary time and $Q_m = \gamma\varepsilon/(\rho\sigma)$ is the minimum flow rate; $Oh = \mu/\sqrt{\rho\gamma d}$ is the Ohnesorge number, and $Bo_e = \varepsilon_0 V^2/(\gamma d)$ is the electric Bond number.

In our experimental system with $\varepsilon/\varepsilon_0 \gg 1$ (high permittivity), $t_e/t_c \ll 1$ (high conductivity), $Oh \ll 1$ (low viscosity), $L/d \gg 1$ (large electrode separation) and $Bo_e \sim 1$ (around the Taylor voltage), the functional dependence in (A 2) is further

reduced to

$$\frac{f}{f_c} \approx F_2\left(\frac{Q_s}{Q_m}\right), \tag{A 3}$$

which is a generalized form of (2.5). Although it is difficult to rigorously justify the dramatic reduction to the form of (A 3), the dimensional analysis offers a guideline for the parametric regime of validity for our model. For example, the Ohnesorge number is no longer small for a highly viscous liquid such as glycerol, in which case the simplified equation (A 3) is no longer valid. In another example, although the electric Bond number is neglected in the simplified model, its influence is manifested by the voltage dependence (secondary compared to the flow rate dependence) of the conical oscillation frequency in figure 3.

There are many simplifications implied in (A 1), the starting point of our dimensional analysis. The surrounding air is assumed to act only as a passive dielectric medium, although it may play an additional hydrodynamic and/or electrostatic role, e.g. by partially stipulating the charge loss ratio ($\Delta q/q_R$). Another simplification is the employment of only one length scale, the nozzle diameter (d), to characterize the Taylor cone. The jet diameter may be additionally needed to fully characterize the cone-jet transition, which will affect the evaluation of the viscous effects (Oh), among other things. Future studies are warranted on these theoretical limitations as well as the parametric regime of validity for our scaling model in (2.5).

REFERENCES

ALEXANDER, M., PAINE, M. & STARK, J. 2006 Pulsation modes and the effect of applied voltage on current and flow rate in nanoelectrospray. *Analyt. Chem.* **78**, 2658.

CHEN, C. 2011 Electrohydrodynamic stability. In *Electrokinetics and Electrohydrodynamics in Microsystems* (ed. A. Ramos). pp. 177–220. Springer.

CHEN, C., SAVILLE, D. & AKSAY, I. 2006*a* Electrohydrodynamic 'drop-and-place' particle deployment. *Appl. Phys. Lett.* **88**, 154104.

CHEN, C., SAVILLE, D. & AKSAY, I. 2006*b* Scaling laws for pulsed electrohydrodynamic drop formation. *Appl. Phys. Lett.* **89**, 124103.

CHOI, H., PARK, J., PARK, O., FERREIRA, P., GEORGIADIS, J. & ROGERS, J. 2008 Scaling laws for jet pulsations associated with high-resolution electrohydrodynamic printing. *Appl. Phys. Lett.* **92**, 123109.

CHOWDHURY, S. & CHAIT, B. 1991 Method for the electrospray ionization of highly conductive aqueous solutions. *Analyt. Chem.* **63**, 1660.

CLOUPEAU, M. & PRUNET-FOCH, B. 1989 Electrostatic spraying of liquids in cone-jet mode. *J. Electrostat.* **22**, 135.

CLOUPEAU, M. & PRUNET-FOCH, B. 1994 Electrohydrodynamic spraying functioning modes: a critical review. *J. Aerosol Sci.* **25**, 1021.

FERNANDEZ DE LA MORA, J. 1996 On the outcome of the coulombic fission of a charged isolated drop. *J. Colloid Interface Sci.* **178**, 209.

FERNANDEZ DE LA MORA, J. 2007 The fluid dynamics of Taylor cones. *Annu. Rev. Fluid Mech.* **39**, 217.

FERNANDEZ DE LA MORA, J. & LOSCERTALES, I. 1994 The current emitted by highly conducting Taylor cones. *J. Fluid Mech.* **260**, 155.

GANAN-CALVO, A., DAVILA, J. & BARRERO, A. 1997 Current and droplet size in the electrospraying of liquids. Scaling laws. *J. Aerosol Sci.* **28**, 249.

JURASCHEK, R. & ROLLGEN, F. 1998 Pulsation phenomena during electrospray ionization. *Intl J. Mass. Spectrom.* **177**, 1.

LORD, RAYLEIGH 1882 On the equilibrium of liquid conducting masses charged with electricity. *Phil. Mag.* **14**, 184.

LU, Y., ZHOU, F., SHUI, W., BIAN, L., GUO, Y & YANG, P. 2001 Pulsed electrospray for mass spectrometry. *Analyt. Chem.* **73**, 4748.

MARGINEAN, I., NEMES, P., PARVIN, L. & VERTES, A. 2006 How much charge is there on a pulsating Taylor cone? *Appl. Phys. Lett.* **89**, 064104.

MARGINEAN, I., NEMES, P. & VERTES, A. 2007 Astable regime in electrosprays. *Phys. Rev.* E **76**, 026320.

PAINE, M. 2009 Transient electrospray behaviour following high voltage switching. *Microfluid Nanofluid* **6**, 775.

PARK, J., HARDY, M., KANG, S., BARTON, K., ADAIR, K., MUKHOPADHYAY, D., LEE, C., STRANO, M., ALLEYNE, A, GEORGIADIS, J., FERREIRA, P. & ROGERS, J. 2007 High resolution electrohydrodynamic jet printing. *Nat. Mater.* **6**, 782.

PARVIN, L., GALICIA, M., GAUNTT, J., CARNEY, L., NGUYEN, A., PARK, E., HEFFERNAN, L. & VERTES, A. 2005 Electrospray diagnostics by Fourier analysis of current oscillations and fast imaging. *Analyt. Chem.* **77**, 3908.

STACHEWICZ, U., DIJKSMAN, J., YURTERI, C. & MARIJNISSEN, J. 2010 Volume of liquid deposited per single event electrospraying controlled by nozzle front surface modification. *Microfluid Nanofluid* **9**, 635.

STACHEWICZ, U., YURTERI, C., MARIJNISSEN, J. & DIJKSMAN, J. 2009 Stability regime of pulse frequency for single event electrospraying. *Appl. Phys. Lett.* **95**, 224105.

TAYLOR, G. 1964 Disintigration of water drops in an electric field. *Proc. R. Soc. Lond.* A **280**, 383.

WEI, J., SHUI, W, ZHOU, F., LU, Y., CHEN, K., XU, G. & YANG, P 2002 Naturally and externally pulsed electrospray. *Mass Spectrom. Rev.* **21**, 148.

WILM, M. & MANN, M. 1994 Electrospray and Taylor-cone theory. Dole's beam of macromolecules at last? *Intl J. Mass Spectrom.* **136**, 167.

XU, S. 2010 Operating regimes of self-regulated electrohydrodynamic cone-jets. MS thesis, Duke University.

YOGI, O., KAWAKAMI, T., YAMAUCHI, M., YE, J. & ISHIKAWA, M. 2001 On-demand droplet spotter for preparing pico- to femtoliter droplets on surfaces. *Analyt. Chem.* **73**, 1896.

ZHAO, Y., BOREYKO, J., CHIANG, M., BAKER, C. & CHEN, C. 2009. Beetle inspired electrospray vapour chamber. *Proceedings of the 2nd International Conference on Micro/Nanoscale Heat and Mass Transfer, Shanghai, China*, Vol. 3, pp. 439-441.